Journal of Nuclear Medicine, published on May 26, 2016 as doi:10.2967/jnumed.116.174300

(2*S*)-2-(3-(1-Carboxy-5-(4-[^{211}At]astatobenzamido)pentyl)ureido)-pentanedioic acid for PSMA-Targeted α-Particle Radiopharmaceutical Therapy

Ana P. Kiess,[1*] Il Minn,[2*] Ganesan Vaidyanathan,[3] Robert F. Hobbs,[1] Anders Josefsson,[2] Colette Shen,[1] Mary Brummet,[2] Ying Chen,[2] Jaeyeon Choi,[3] Eftychia Koumarianou,[3] Kwamena Baidoo,[4] Martin W. Brechbiel,[4] Ronnie C. Mease,[2] George Sgouros,[2] Michael R. Zalutsky,[3] Martin G. Pomper[1,2]

[1]Department of Radiation Oncology and Molecular Radiation Sciences; [2]Russell H. Morgan Department of Radiology and Radiological Science, Johns Hopkins University School of Medicine, Baltimore, MD; [3]Department of Radiology, Duke University Medical Center, Durham, NC; [4]Center for Cancer Research, National Cancer Institute, Bethesda, MD; *Authors contributed equally.

Address Correspondence to:

Martin G. Pomper, M.D., Ph.D.
Johns Hopkins Medical School
1550 Orleans Street, 492 CRB II
Baltimore, MD 21287
Email: mpomper@jhmi.edu
Phone: 443-956-5055
Fax: 443-817-0990

ABSTRACT

Introduction: Alpha particle emitters have a high linear energy transfer and short range, offering the potential for treating micrometastases while sparing normal tissues. We developed a urea-based, ^{211}At-labeled small-molecule targeting prostate-specific membrane antigen (PSMA) for treatment of micrometastases due to prostate cancer (PC).

Methods: PSMA-targeted (2*S*)-2-(3-(1-carboxy-5-(4-[^{211}At]astatobenzamido)pentyl)ureido)-pentanedioic acid ([^{211}At]**6**) was synthesized. Cellular uptake and clonogenic survival were tested in PSMA-positive (PSMA+) PC3 PIP and PSMA-negative (PSMA-) PC3 flu human PC cells after [^{211}At]**6** treatment. Anti-tumor efficacy of [^{211}At]**6** was evaluated in mice bearing PSMA+ PC3 PIP and PSMA- PC3 flu flank xenografts at a 740 kBq dose, and in mice bearing PSMA+, luciferase-expressing PC3-ML micrometastases. Biodistribution was determined in mice bearing PSMA+ PC3 PIP and PSMA- PC3 flu flank xenografts. Sub-organ distribution was evaluated using α-Camera images, and micro-scale dosimetry was modeled. Long-term toxicity was assessed in mice for 12 mo.

Results: [^{211}At]**6** treatment resulted in PSMA-specific cellular uptake and decreased clonogenic survival in PSMA+ PC3 PIP cells, and caused significant tumor growth delay in PSMA+ PC3 PIP subcutaneous tumors. Significantly improved survival was achieved in the newly developed PSMA+ micrometastatic PC model. Biodistribution showed uptake of [^{211}At]**6** in PSMA+ PC3 PIP tumors and in kidneys. Micro-scale kidney dosimetry based on α-Camera images and a nephron model revealed hot spots in the proximal renal tubules. Long-term toxicity studies confirmed that the dose-limiting toxicity was late radiation nephropathy.

Conclusion: PSMA-targeted [^{211}At]**6** α-particle radiotherapy yielded significantly improved survival in mice bearing PC micrometastases after systemic administration. [^{211}At]**6** also

showed uptake in renal proximal tubules resulting in late nephrotoxicity, highlighting the importance of long-term toxicity studies and micro-scale dosimetry.

INTRODUCTION

A significant fraction of men with prostate cancer (PC) develop metastatic disease with attendant consequences (*1, 2*). For example, metastatic bone disease carries a 40% one-year survival rate. An important group of patients to address with targeted radiopharmaceutical therapy (RPT) are those with biochemical recurrence and no imaging findings, namely, micrometastatic disease. Some of those patients will have stable disease on hormonal therapy for years but many will progress to castration-resistant prostate cancer (CRPC), with limited treatment options. Systemic agents including docetaxel, enzalutamide, and abiraterone have provided small survival benefits (*3, 4*). The recent Phase III ALSYMPCA trial of Xofigo® ($^{223}RaCl_2$) demonstrated the feasibility of α-emitter RPT in CRPC (*5*). However, survival benefit was only 3 mo and therapeutic effect was limited to bone metastases. To expand beyond the success of Xofigo® we developed [^{211}At]**6**, a urea-based α-emitter that targets prostate-specific membrane antigen (PSMA), which is over-expressed > 1,000-fold relative to normal prostate in nearly all PC and is present in solid tumor neovasculature (*6-8*). Based on clinical studies with PSMA-targeted imaging agents (*9, 10*), both bone and soft tissue metastases should be treatable by targeting PSMA. Moreover, the peri-nuclear localization of PSMA enhances tumor cell kill (*11*).

PSMA-targeted RPT has been confined to β^--emitters including clinical studies with [^{131}I]MIP1466 (*12*) and ^{177}Lu-labeled J591, which was dose-limited by myelosuppression, particularly thrombocytopenia (*13*). Alpha-particles have clear advantages over β-particles for treatment of micrometastases, including a high linear energy transfer (LET) and a short tissue range (*14*), which should facilitate selective eradication of small clusters of malignant cells while sparing surrounding normal tissue. In addition to the ALSYMPCA trial for CRPC, α-particle emitters have been investigated in other clinical trials and have consistently shown only mild

toxicities (*15*). Among the α-emitters, ^{211}At has particularly favorable characteristics for clinical development including a 7.2-h half-life that is well matched to small molecule therapeutics (*16*). A detailed review (*17*) summarizes the current status of ^{211}At-labeled radiotherapeutics and the importance for understanding the micro-scale distribution of α-emitters to predict toxicity and efficacy, an essential aspect of our studies.

MATERIALS AND METHODS

Chemistry

Compounds **1** and **2** (**Scheme 1**) were prepared by the method of Chen et al. and Maresca et al., respectively (*18, 19*). Stannane **3** was prepared as previously described (*18*). Details regarding the synthesis of **4** and radiochemistry are presented in **Supplemental Data**.

In Vitro Studies

Cell lines and culture conditions. The isogenic human PC3 cell lines PIP (PSMA-positive) and flu (PSMA-negative) were originally obtained from Dr. Warren Heston (Cleveland Clinic) and were maintained as described (*20*). The androgen-independent PC3 cell line was originally derived from a human CRPC bone metastasis. The PSMA+ PC3 PIP line was stably transfected to over-express PSMA. Parental PC3-ML-Luc cells were obtained from Dr. Mauricio Reginato (Drexel University).

*Paired-label uptake of [^{131}I]**5** and [^{211}At]**6***. Both PSMA+ PC3 PIP and PSMA- PC3 flu cells were plated at a density of 5 × 10^5 cells/well and incubated overnight. Cells were then incubated in

solutions of [^{131}I]**5** and [^{211}At]**6** in medium (~3.7 kBq/100 µL) at 37°C for 0.5, 1, 2 and 4 h. Cell culture supernatants were then removed and cells were washed twice with PBS. Cells were solubilized by incubation with 1 M NaOH (2 × 2 mL) for 10 min. Aliquots (100 µL) of cell culture supernatants, solubilized cells and input dose standards were counted for ^{131}I and ^{211}At activity in an LKB Wallac 1282 γ-counter (Perkin-Elmer, Waltham, MA), and cell-associated radioactivity as percentage of input dose was calculated. In a parallel assay, PSMA+ PC3 PIP cells were co-incubated with the two radiotracers and (*R,S*)-2-(phosphonomethyl)pentanedioic acid (2-PMPA; 100 µM final concentration) (*21*).

In vitro cytotoxicity. PSMA+ PC3 PIP cells were incubated in triplicate flasks at a density of 5 × 10^3 cells at 37°C for 3 d. Cells were replenished with fresh medium (control) or varying concentrations of [^{211}At]astatide or [^{211}At]**6**, and incubated at 37°C. After 10 d, the cells were washed with PBS, fixed for 5 min with 95% ethanol, stained with 0.4% trypan blue, and washed again with PBS. Colonies were counted using a Darkfield Quebec Colony Counter (Cambridge Instruments, Buffalo, NY). The D_0 and 90% confidence limits of the regression fit were determined using Sigma Plot (Jandel Scientific, San Rafael, CA).

In Vivo Studies

*Paired-label biodistribution of [^{131}I]**5** and [^{211}At]**6***. All animal experiments were performed following the guidelines established by the Duke and Johns Hopkins University Institutional Animal Care and Use Committees. Six- to eight-week-old, athymic mice weighing ~25 g (Charles River) were injected with 10^6 PSMA+ PC3 PIP cells into one flank and 10^6 PSMA- PC3 flu cells into the opposite flank. Biodistribution studies were conducted when the xenografts were 300-500 mm^3 in size. Mice received 0.2 MBq of each radiotracer *via* tail vein and groups

of five mice were sacrificed 0.5, 1, 2, 4 and 18 h post-injection. Tissues were isolated, weighed and counted for ^{131}I and ^{211}At. Percentages of injected dose per organ and per gram of tissue were computed. Differences in tissue uptake between the two radiotracers was calculated using a two-tailed, paired Student's t-test.

Anti-tumor efficacy in flank xenograft model. Cells were grown to 80–90% confluence before trypsinization and formulation in RPMI for inoculation. Male athymic mice weighing ~20 g were injected subcutaneously within the flank with 1 x 10^6 PSMA+ PC3 PIP or PSMA- PC3 flu cells. Treatments were administered 7–12 d later when tumor volume was less than 200 mm^3. Animals (n = 9-11 per group) received 740 kBq [^{211}At]**6** intravenously or were untreated. Tumors were then measured 2-3 times per week until they reached 10× pre-treatment volume. The probability of reaching 10× initial tumor volume was characterized using Kaplan-Meier curves, and comparison was performed using the log-rank test (Graphpad Prism, La Jolla, CA).

Antitumor efficacy in micrometastatic model. To generate a PSMA-expressing metastatic PC model, PC3-ML-Luc cells (*22*) were infected with lentiviral particles as described (*23*). After infection, cells were stained with YC-36, a PSMA-targeted small molecule conjugated with fluorescein isothiocyanate (*11*). PSMA-positive single cells were sorted using the MoFlo (DakoCytomation, Glostrup, Denmark) and clones were established. The metastatic potential of each clone was tested by monitoring the development of metastases and progression by in vivo bioluminescence imaging (BLI) (IVIS Spectrum, Perkin-Elmer) following intravenous injection of 1 × 10^6 cells. Four- to six-week-old NOG (NOD/Shi-*scid*/IL-2Rγ^{null}) mice (Animal Resources Core, Johns Hopkins) were injected with 1 x 10^6 PC3-ML-Luc-PSMA cells. One day later, mice

(n = 5/group) were injected intravenously with 37, 111, 185, or 370 kBq [^{211}At]**6**. Metastatic tumor progression was monitored by in vivo BLI and survival.

Toxicity and maximum tolerated dose. The maximum tolerated dose was defined as the highest dose at which no animal died or lost more than 20% of its pre-treatment weight. Non-tumor-bearing CD1 mice (Charles River, n = 10/group) weighing 25-30 g received intravenous injections of 0, 37, 111, 370, 740, or 1,480 kBq [^{211}At]**6**, and then were weighed and inspected twice per week for at least 12 mo. Urinalysis was performed monthly for each animal. Upon sacrifice, animals were evaluated by the Johns Hopkins Department of Comparative Pathology with serum metabolic panel, blood counts, and full necropsy including detailed histopathology of kidney.

*[^{211}At]**6** tumor and kidney biodistribution for dosimetry***.*** Male athymic mice weighing ~20 g were injected subcutaneously in the right and left flank areas with 10^6 PSMA+ PC3 PIP and 10^6 PSMA- PC3 flu cells, respectively. Eight mice were injected intravenously with 3.7 MBq [^{211}At]**6** and sacrificed at 1 (n=3), 4 (n=3), 8 (n=1) and 16 h (n=1). The left kidney and both tumors were harvested, weighed, and activity was measured using a 1282 Compugamma γ-counter (Pharmacia, Gaithersburg, MD).

α-Camera imaging. Digital autoradiography imaging was performed using the α-Camera (*24*) to determine the activity concentration and distribution of [^{211}At]**6** at sub-tissue levels. Kidney and tumors were frozen in dry ice and cryostat-sectioned in 8 μm sections. Consecutive sections were taken for hematoxylin and eosin staining and α-Camera imaging for 15-20 min. The α-

Camera imaging samples were also measured in the γ-counter to allow image quantification. Regions of interest (ROIs) were drawn using ImageJ Fiji version 1.49g (NIH) to measure activity levels within the different compartments. In addition, the relative [^{211}At]**6** activity concentrations in the sub-tissue level versus the average of the whole tissue sample was calculated.

Dosimetry. Whole body and small-scale kidney/tumor dosimetry for [^{211}At]**6** was derived from the biodistribution data and quantified α-Camera images, respectively. Details regarding whole body dosimetry are provided in **Supplemental Data**. For small-scale kidney dosimetry, histologically verified ROIs corresponding to proximal tubules and glomeruli were drawn on α-Camera images and integrated over time to obtain the total number of decays. Micro-scale S-values for ^{211}At decays in these regions were multiplied by the total number of decays to yield the absorbed doses to proximal tubules and glomeruli. The S-values were calculated according to a previously created Monte Carlo based kidney nephron model (*25*).

Small-scale tumor dosimetry was done by obtaining histograms of activity uptake per time point with a same number of bins, ranking the bins by uptake and integrating over bins with the same ranking from time point to time point to obtain a time-integrated activity histogram. Absorbed fractions for self-dose and neighbor-dose for pixels (voxels) were calculated using GEANT4 Monte Carlo simulation. Activity in adjacent bins was randomly determined for each bin and the S-values applied to obtain a normalized dose volume histogram.

RESULTS

Radiochemistry

[^{131}I]**5** was synthesized in similar radiochemical yields as obtained with ^{125}I (*18*). Astatodestannylation and in situ deprotection of **3** or **4** (**Scheme 1**) delivered [^{211}At]**6** in 62.6 ± 9.5% (n = 23) radiochemical yield using **3** in >98% radiochemical purity as determined by high performance liquid chromatography (HPLC). Co-injection with non-radioactive **5** (iodinated) showed that both eluted with the same retention time on HPLC. No co-eluting carrier peak was observed on HPLC with [^{211}At]**6**.

In Vitro Studies

The percent uptake in PSMA+ PC3 PIP cells increased from 5.0 ± 0.3 (^{131}I) and 4.9 ± 0.3 (^{211}At) at 0.5 h to 22.4 ± 1.1 (^{131}I) and 19.3 ± 1.0 (^{211}At) at 4 h (**Figure 1A**, top panel). The uptake of [^{211}At]**6** was lower than [^{131}I]**5**. PSMA specificity of uptake was demonstrated by its reduction to <2% of input dose when co-incubated with the PSMA inhibitor 2-PMPA (*21*) (**Figure 1A**, middle panel). Moreover, uptake in PSMA- PC3 flu cells was significantly lower than in PSMA+ PC3 PIP cells (**Figure 1A**, bottom panel). The clonogenic survival of PSMA+ PC3 PIP cells following incubation with [^{211}At]astatide and [^{211}At]**6** for 4 h is shown in **Figure 1B**. A D_0 of 118.4 kBq/mL was obtained for [^{211}At]**6** compared to 244.2 kBq/mL for [^{211}At]astatide.

In Vivo Studies

Biodistribution. Uptake of ^{131}I and ^{211}At in PSMA+ PC3 PIP and PSMA- PC3 flu tumors after injection of [^{131}I]**5** and [^{211}At]**6** is presented in **Figure 2**. Paired-label studies are of value as both tracers are subjected to identical conditions so that each experiment has its own control (*26, 27*). In addition, in the case of ^{211}At-labeled compounds, in vivo stability is a major concern and the paired-label biodistribution studies can shed some light on the potential effects of lower carbon-halogen bond strength on biodistribution (*28*). As seen in cell culture, tumor uptake

increased for both agents with time and was higher for [^{131}I]**5**. Except at 18 h, the difference in the uptake between the two radiotracers was significant. Maximum tumor uptake of 41.5 ± 18.4% ID/g for [^{131}I]**5** and 31.1 ± 9.8% ID/g for [^{211}At]**6** was seen at 18 h. With both radiotracers, uptake was significantly lower in PSMA- PC3 flu xenografts.

Uptake of ^{131}I and ^{211}At in normal tissues is given in **Supplemental Tables S1** and **S2**, respectively. Uptake in kidney was high for both radiotracers. However, the renal uptake of ^{211}At was only 50-70% of that observed for ^{131}I at all time points. The uptake from [^{211}At]**6** in thyroid, lungs and stomach was higher than that from [^{131}I]**5** suggesting a higher degree of dehalogenation for [^{211}At]**6**. PSMA+ PC3 PIP tumor-to-normal tissue ratios generally increased with time (**Figure 3**). Except for in the spleen and kidneys, the tumor-to-tissue ratio was higher for [^{131}I]**5**.

Anti-tumor efficacy. Nude mice bearing PSMA+ PC3 PIP flank tumors had significant tumor growth delay after treatment with 740 kBq [^{211}At]**6** compared with other groups (**Figure 4**). Tumors from 2 of 11 treated animals harboring PSMA+ PC3 PIP xenografts disappeared and did not recur during the 8-mo study. Median times to reach 10× tumor volume for PSMA+ PC3 PIP (treated), PSMA+ PC3 PIP (untreated), PSMA- PC3 flu (treated), and PSMA- PC3 flu (untreated) were 35, 19, 24, and 19 d, respectively. The difference among treatment groups was statistically significant (P = 0.01) by the log-rank test. Individual animal tumor volume plots are shown in **Supplemental Figure S1**.

Antitumor efficacy in a micrometastatic model. NOG mice injected with PC3-ML-Luc-PSMA developed metastases within liver, kidney, and bone (**Supplemental Figure S2**). Untreated

animals died within 7-8 weeks after receiving cells. Median survival was 58, 59, 72, 97, and 110 days for those untreated and those receiving 37, 111, 185, and 370 kBq, respectively (**Figure 5** and **Supplemental Figure S3**). Survival rates were statistically different among groups (P < 0.0001).

In vivo toxicity and maximum tolerated dose. The maximum tolerated single dose of [^{211}At]**6** in immunocompetent CD1 mice was 37 kBq. The dose-limiting toxicity was late radiation nephropathy. At 1.5 MBq all animals developed proteinuria 1-2 mo post-treatment and died of nephropathy at 3-9 mo post-treatment (**Supplemental Figure S4**). Toxicity appeared later in the lower dose groups. After treatment with 740, 370 and 111 kBq, 9/10, 7/10, and 2/10 animals died by 12 mo post-treatment, respectively. Animals treated with 37 kBq developed mild proteinuria that later resolved.

Necropsy for all deceased mice showed nephropathy consistent with radiation from α-particles. The average size of the kidneys in mice treated with 1.5 MBq [^{211}At]**6** was 0.11 g compared with 0.26 g for controls, average blood urea nitrogen was 248 mg/dL (normal range 19-32 mg/dL), average creatinine was 1.4 mg/dL (normal <0.6 mg/dL), and average calcium was 12.7 mg/dL (normal 9.7-11.2 mg/dL). On histopathology, there was subcortical atrophy with prominent degenerative loss of the proximal tubules, tubular ectasia and proteinosis (**Figure 6**). No animals died of acute or chronic hematologic toxicity, but average hemoglobin at necropsy was 7.8 g/dL (normal 15.4-17.2 g/dL) likely reflecting anemia due to reduced erythropoietin from nephropathy.

*[^{211}At]**6** tumor and kidney biodistribution for dosimetry.* [^{211}At]**6** biodistribution for kidneys, PSMA+ PC3 PIP and PSMA- PC3 flu tumors after a 3.7 MBq dose are shown in **Supplemental**

Figure S5. The highest kidney uptake of [^{211}At]**6** occurred at 4 h (97.8 ± 12.2 %ID/g) while the the highest uptake in PSMA+ PC3 PIP tumors occurred at 16 h (28.2 %ID/g). For the PSMA- PC3 flu tumors, maximum uptake was at 1 h (2.1 ± 1.4 %ID/g).

α-Camera imaging. More than 91% of the activity in the kidney was localized to the cortex at all time points (**Figure 7**). Hot spots were histologically verified to correspond to the proximal tubules, and had activity concentrations 3.5-4.5 times higher than the entire kidney section average. In PSMA+ tumors there were heterogeneous hot spots of activity measuring 3.8, 3.0, 2.5 and 2.5 times higher than the entire tumor section average at 1, 4, 8 and 16 h, respectively, suggesting transition toward a more homogeneous tumor distribution with time.

Dosimetry. Whole organ kidney/tumor dosimetry for [^{211}At]**6** was based on the biodistribution data shown in **Supplemental Figure S5**. Considering only the α-emissions and assuming local deposition within the kidney and tumors, the mean absorbed dose of [^{211}At]**6** was 24.6, 10.0 and 0.44 mGy/kBq for the kidney, PSMA+ PC3 PIP and PSMA- PC3 flu tumors, respectively. When the activity concentration and distribution derived from the quantified α-Camera images were inserted in the nephron model for 1 MBq [^{211}At]**6**, an absorbed dose up to 123 Gy in portions of the proximal tubules was determined. This is about 5-fold higher compared with the mean to the whole kidney and higher than glomerular doses (which were up to 42 Gy including self-dose and contribution from neighboring tubules). For the PSMA+ PC3 PIP tumor small-scale dosimetry, using the integrated activity and dose volume histograms, the dose per bin ranged from 0.26-36 Gy, for an average dose of 10 Gy and a root mean square of 5.5 Gy. The variability in uptake in the tumor gave an equivalent uniform dose of 6.9 Gy.

DISCUSSION

We feature [^{211}At]**6** in the context of a new paradigm for development of ^{211}At-labeled small-molecule PSMA inhibitors for α-RPT of PC. Treatment with [^{211}At]**6** resulted in PSMA-specific cellular uptake and decreased clonogenic survival in vitro. This agent also offered significant tumor growth delay in a PSMA+ PC3 PIP flank xenograft model and significantly improved survival in a new PSMA+ micrometastatic PC model. Biodistribution studies showed uptake of [^{211}At]**6** in PSMA+ PC3 PIP tumors and in kidneys. Micro-scale kidney dosimetry based on α-Camera images and a nephron model revealed hot spots in the proximal renal tubules, and long-term toxicity studies confirmed that the dose-limiting toxicity was late radiation nephropathy with loss of the proximal tubules.

The recent success of $^{223}RaCl_2$, which showed survival benefit and minimal toxicity in patients with CRPC, has demonstrated the feasibility of α-particle RPT, but $^{223}RaCl_2$ is limited to treatment of bone metastases. [^{211}At]**6** is in a class of urea-based small molecules that targets PSMA and have shown uptake in pelvic and para-aortic lymph node metastases, prostate, visceral metastastases, and bone metastases in human PC imaging studies (*9, 10*). Accordingly, PSMA-targeted α-particle RPT may be suitable for any PC site, particularly for micrometastatic disease not visible by imaging. Alpha particles have potential advantages for treatment of micrometastatic cancer, including high LET (100 keV/μm for ^{211}At) and short range (3-4 cells) versus β^--emitters. Therefore, they may complement PSMA-targeted β^--emitters such as [^{131}I]MIP1466, ^{177}Lu-labeled J591, and ^{177}Lu-labeled PSMA I&T, under investigation for macroscopic disease (*12, 13, 29*). Previous studies have shown that the scaffold on which [^{211}At]**6** was based has extremely high affinity for PSMA (K_i = 0.01 nM) and that the targeted drug is localized not only to the plasma membrane but also to the peri-nuclear area of the cell, potentially increasing DNA damage (*11*). The potential for treatment of PC micrometastases

with [^{211}At]**6** is particularly supported by the improved survival demonstrated in our PSMA+ micrometastatic PC model (**Figure 5**). This new model is a valuable tool for evaluation of PSMA-targeted therapy and imaging, with metastases developing in the liver, kidney, and bone after injection with PC3-ML-Luc-PSMA cells.

Although the potential for α-particle RPT has been well established, clinical translation of these therapies has been challenging due to limited access to radionuclides, unresolved chemistry, in vivo instability, and need for improved dosimetry modeling. For ^{211}At-labeled agents there is particular concern regarding dehalogenation in vivo. Our biodistribution results demonstrated mild uptake of ^{211}At in thyroid, stomach, spleen, and lungs, consistent with some deastatination (**Figure 3**).

The short range of α-particles may limit toxicity to off-target tissues, but for PSMA-targeted RPT there is concern regarding renal toxicity due to physiologic PSMA expression in the proximal tubules. PSMA expression has been previously demonstrated in human proximal tubules by immunohistochemistry, and PSMA imaging in humans also demonstrates significant renal cortical uptake (*6, 29-31*). Our study confirmed that the dose-limiting toxicity for [^{211}At]**6** was late radiation nephropathy, demonstrated by both histopathology at necropsy and serial laboratory studies (**Figure 6**). The MTD in CD1 mice was 37 kBq and the lethal dose to 10% of mice (LD_{10}) was 111 kBq, which is lower than the LD_{10} for [^{211}At]astatide (555 kBq) in mice (*32*). Those toxicity results are consistent with the macro- and micro-level biodistribution and dosimetry modeling discussed below, emphasizing the importance of long-term toxicity studies and comprehensive dosimetry for characterization and translation of α-particle RPT. To widen the therapeutic window for PSMA-targeted α-particle RPT, we are currently investigating other

urea-based agents with more favorable tumor-to-kidney dose ratios. Of note, our small molecule [^{211}At]**6** did not show significant acute hematologic toxicity, in contrast to high-molecular-weight RPTs such as antibodies that typically have dose-limiting hematologic toxicity.

α-Camera images (**Figure 7**) highlight the value of microscale dose calculations, particularly for short-range α-emitters. Microscale dosimetry gave an absorbed dose to the critical sub-structure of the kidneys that was 5 times greater than the average whole kidney dose. The factor of 5 seems high given that the hot spot uptake is less than five at all time points. However, the model allows for a non-trivial empty lumen space that does not carry the activity, therefore the dose can be greater in the model than a straightforward "hot spot" calculation. It is possible that with more sophisticated parameterization of the kidney, more accurate S-values might be obtained. Concerning the distribution and shape of the hot spot activity, it is apparent that the hot spots do not cover the entire lengths of the tubules, which are convoluted and pass in and out of the tissue section planes. The likely explanation is that after passing through the glomeruli, [^{211}At]**6** attaches to the nearest portion of the proximal tubule and does not span the full length of the tubules.

CONCLUSION

PSMA-targeted α-particle RPT with [^{211}At]**6** resulted in specific PC cell kill in vitro and in vivo after systemic administration, showing promise for treatment of PC micrometastases. It also showed uptake in renal proximal tubules resulting in late nephrotoxicity, highlighting the importance of long-term toxicity studies and micro-scale dosimetry. Other agents are being developed with more favorable tumor-to-kidney dose ratios.

DISCLOSURE

This work was supported by NIH CA116477, CA184228, CA134675, CA183031, CA157542, and EB005324 and in part by the Intramural Research Program of the NIH, National Cancer Institute, Center for Cancer Research. No other potential conflict of interest relevant to this article was reported.

ACKNOWLEDGMENTS

We thank Dr. Warren Heston for providing the PSMA+ PC3 PIP and PSMA- PC3 flu cells, and Dr. Mauricio Reginato for the PC3-ML-Luc cells.

REFERENCES

1. American Cancer Society. Cancer Facts & Figures 2012. *Atlanta: American Cancer Society.* 2012.

2. Antonarakis ES, Feng Z, Trock BJ, et al. The natural history of metastatic progression in men with prostate-specific antigen recurrence after radical prostatectomy: long-term follow-up. *BJU international.* Jan 2012;109(1):32-39.

3. de Bono JS, Logothetis CJ, Molina A, et al. Abiraterone and increased survival in metastatic prostate cancer. *The New England journal of medicine.* May 26 2011;364(21):1995-2005.

4. de Bono JS, Oudard S, Ozguroglu M, et al. Prednisone plus cabazitaxel or mitoxantrone for metastatic castration-resistant prostate cancer progressing after docetaxel treatment: a randomised open-label trial. *Lancet.* Oct 2 2010;376(9747):1147-1154.

5. Parker C, Heinrich D, O'Sullivan JM, et al. Overall survival benefit of radium-223 chloride (AlpharadinTM) in the treatment of patients with symptomatic bone metastases in castration-resistant prostate cancer (CRPC): A phase III randomized trial (ALSYMPCA). *Eur J Cancer.* 2011;47(Supp 2):3.

6. Silver DA, Pellicer I, Fair WR, Heston WD, Cordon-Cardo C. Prostate-specific membrane antigen expression in normal and malignant human tissues. *Clin Cancer Res.* Jan 1997;3(1):81-85.

7. Chang SS, O'Keefe DS, Bacich DJ, Reuter VE, Heston WD, Gaudin PB. Prostate-specific membrane antigen is produced in tumor-associated neovasculature. *Clin Cancer Res.* Oct 1999;5(10):2674-2681.

8. Foss CA, Mease RC, Cho SY, Kim HJ, Pomper MG. GCPII imaging and cancer. *Current medicinal chemistry.* 2012;19(9):1346-1359.

9. Rowe SP, Macura KJ, Ciarallo A, et al. Comparison of Prostate-Specific Membrane Antigen-Based 18F-DCFBC PET/CT to Conventional Imaging Modalities for Detection of Hormone-Naive and Castration-Resistant Metastatic Prostate Cancer. *Journal of nuclear medicine.* Jan 2016;57(1):46-53.

10. Eiber M, Maurer T, Souvatzoglou M, et al. Evaluation of Hybrid 68Ga-PSMA Ligand PET/CT in 248 Patients with Biochemical Recurrence After Radical Prostatectomy. *Journal of nuclear medicine.* May 2015;56(5):668-674.

11. Kiess AP, Minn I, Chen Y, et al. Auger Radiopharmaceutical Therapy Targeting Prostate-Specific Membrane Antigen. *Journal of nuclear medicine.* Sep 2015;56(9):1401-1407.

12. Hillier S, Rubino K, Maresca K, et al. [131I]MIP-1466, a small molecule prostate-specific membrane antigen (PSMA) inhibitor for targeted radiotherapy of prostate cancer. *Journal of nuclear medicine.* 2012;53(Supp1):170.

13. Tagawa ST, Beltran H, Vallabhajosula S, et al. Anti-prostate-specific membrane antigen-based radioimmunotherapy for prostate cancer. *Cancer.* Feb 15 2010;116(4 Suppl):1075-1083.

14. Mulford DA, Scheinberg DA, Jurcic JG. The promise of targeted {alpha}-particle therapy. *Journal of nuclear medicine.* Jan 2005;46 Suppl 1:199S-204S.

15. Larson SM, Carrasquillo JA, Cheung NK, Press OW. Radioimmunotherapy of human tumours. *Nature reviews Cancer.* Jun 2015;15(6):347-360.

16. Guerard F, Gestin JF, Brechbiel MW. Production of [(211)At]-Astatinated Radiopharmaceuticals and Applications in Targeted alpha-Particle Therapy. *Cancer biotherapy & radiopharmaceuticals.* Jan 2013;28(1):1-20.

17. Sgouros G, Roeske JC, McDevitt MR, et al. MIRD Pamphlet No. 22 (abridged): radiobiology and dosimetry of alpha-particle emitters for targeted radionuclide therapy. *Journal of nuclear medicine.* Feb 2010;51(2):311-328.

18. Chen Y, Foss CA, Byun Y, et al. Radiohalogenated prostate-specific membrane antigen (PSMA)-based ureas as imaging agents for prostate cancer. *Journal of medicinal chemistry.* Dec 25 2008;51(24):7933-7943.

19. Maresca KP, Hillier SM, Femia FJ, et al. A series of halogenated heterodimeric inhibitors of prostate specific membrane antigen (PSMA) as radiolabeled probes for targeting prostate cancer. *Journal of medicinal chemistry.* Jan 22 2009;52(2):347-357.

20. Banerjee SR, Foss CA, Castanares M, et al. Synthesis and evaluation of technetium-99m- and rhenium-labeled inhibitors of the prostate-specific membrane antigen (PSMA). *Journal of medicinal chemistry.* Aug 14 2008;51(15):4504-4517.

21. Jackson PF, Cole DC, Slusher BS, et al. Design, synthesis, and biological activity of a potent inhibitor of the neuropeptidase N-acetylated alpha-linked acidic dipeptidase. *Journal of medicinal chemistry.* Jan 19 1996;39(2):619-622.

22. Bhatnagar A, Wang Y, Mease RC, et al. AEG-1 Promoter-Mediated Imaging of Prostate Cancer. *Cancer Res.* Oct 15 2014;74(20):5772-5781.

23. Mukherjee A, Darlington T, Baldwin R, et al. Development and screening of a series of antibody-conjugated and silica-coated iron oxide nanoparticles for targeting the prostate-specific membrane antigen. *ChemMedChem.* Jul 2014;9(7):1356-1360.

24. Back T, Jacobsson L. The alpha-camera: a quantitative digital autoradiography technique using a charge-coupled device for ex vivo high-resolution bioimaging of alpha-particles. *Journal of nuclear medicine.* Oct 2010;51(10):1616-1623.

25. Hobbs RF, Song H, Huso DL, Sundel MH, Sgouros G. A nephron-based model of the kidneys for macro-to-micro alpha-particle dosimetry. *Phys Med Biol.* Jul 7 2012;57(13):4403-4424.

26. Vaidyanathan G, Affleck DJ, Zalutsky MR. Validation of 4-[fluorine-18]fluoro-3-iodobenzylguanidine as a positron-emitting analog of MIBG. *Journal of nuclear medicine.* Apr 1995;36(4):644-650.

27. Pressman D, Day ED, Blau M. The use of paired labeling in the determination of tumor-localizing antibodies. *Cancer Res.* Oct 1957;17(9):845-850.

28. Wilbur DS, Chyan MK, Hamlin DK, et al. Reagents for astatination of biomolecules: comparison of the in vivo distribution and stability of some radioiodinated/astatinated benzamidyl and nido-carboranyl compounds. *Bioconjugate chemistry.* Jan-Feb 2004;15(1):203-223.

29. Weineisen M, Schottelius M, Simecek J, et al. 68Ga- and 177Lu-Labeled PSMA I&T: Optimization of a PSMA-Targeted Theranostic Concept and First Proof-of-Concept Human Studies. *Journal of nuclear medicine.* Aug 2015;56(8):1169-1176.

30. Kinoshita Y, Kuratsukuri K, Landas S, et al. Expression of prostate-specific membrane antigen in normal and malignant human tissues. *World J Surg.* Apr 2006;30(4):628-636.

31. Cho SY, Gage KL, Mease RC, et al. Biodistribution, tumor detection, and radiation dosimetry of 18F-DCFBC, a low-molecular-weight inhibitor of prostate-specific membrane antigen, in patients with metastatic prostate cancer. *Journal of nuclear medicine.* Dec 2012;53(12):1883-1891.

32. McLendon RE, Archer GE, Garg PK, Bigner DD, Zalutsky MR. Radiotoxicity of systematically administered [211At]astatide in B6C3F1 and BALB/c (nu/nu) mice: a long-term survival study with histologic analysis. *Int J Radiat Oncol Biol Phys.* Apr 1 1996;35(1):69-80.

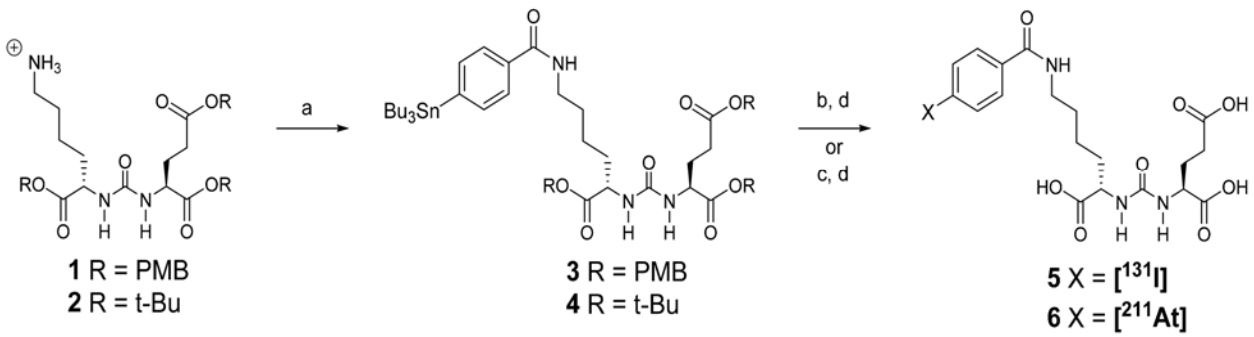

Scheme 1. Synthesis of [^{131}I]**5** and [^{211}At]**6.**

a. N-succinimidyl-4-tributylstannyl benzoate, triethylamine, methylene chloride; b. ^{211}At, *N*-chlorosuccinimide, acetic acid, methanol, room temp 30 min; c. Na[^{131}1]N-chlorosuccinimide, acetic acid, methanol, room temp 30 min; d. TFA/water 50°C 30 min or room temperature 60-90 min. PMB = para-methoxybenzyl.

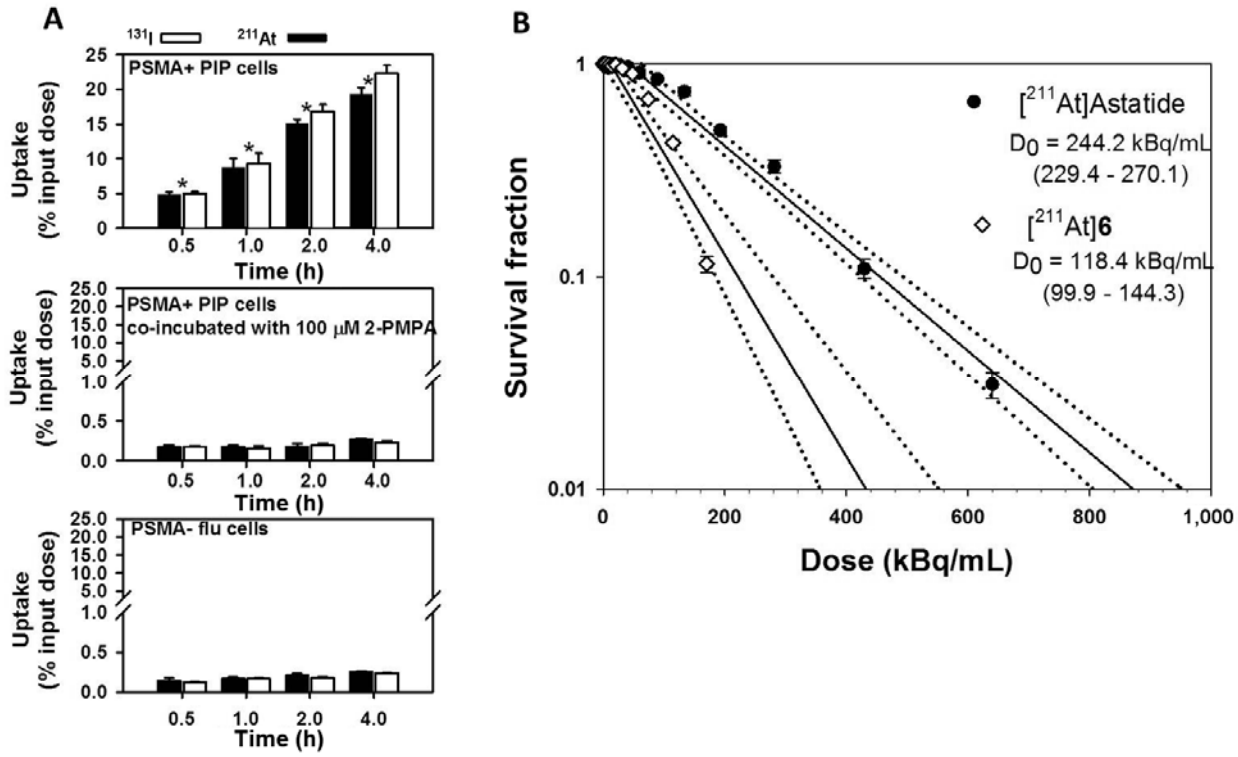

Figure 1. (**A**) Paired-label uptake of [^{131}I]**5** and [^{211}At]**6** in PSMA+ PC3 PIP and PSMA- PC3 flu cells. Uptake in PSMA+ cells also was determined in presence of PSMA inhibitor, 2-PMPA. Values indicate mean ± standard deviation. Asterisks indicate difference between radiotracers using paired t-test (P<.05). (**B**) Clonogenic survival of PSMA+ cells following incubation with [^{211}At]astatide and [^{211}At]**6**. Dashed line indicates 95% confidence limit for regression fit.

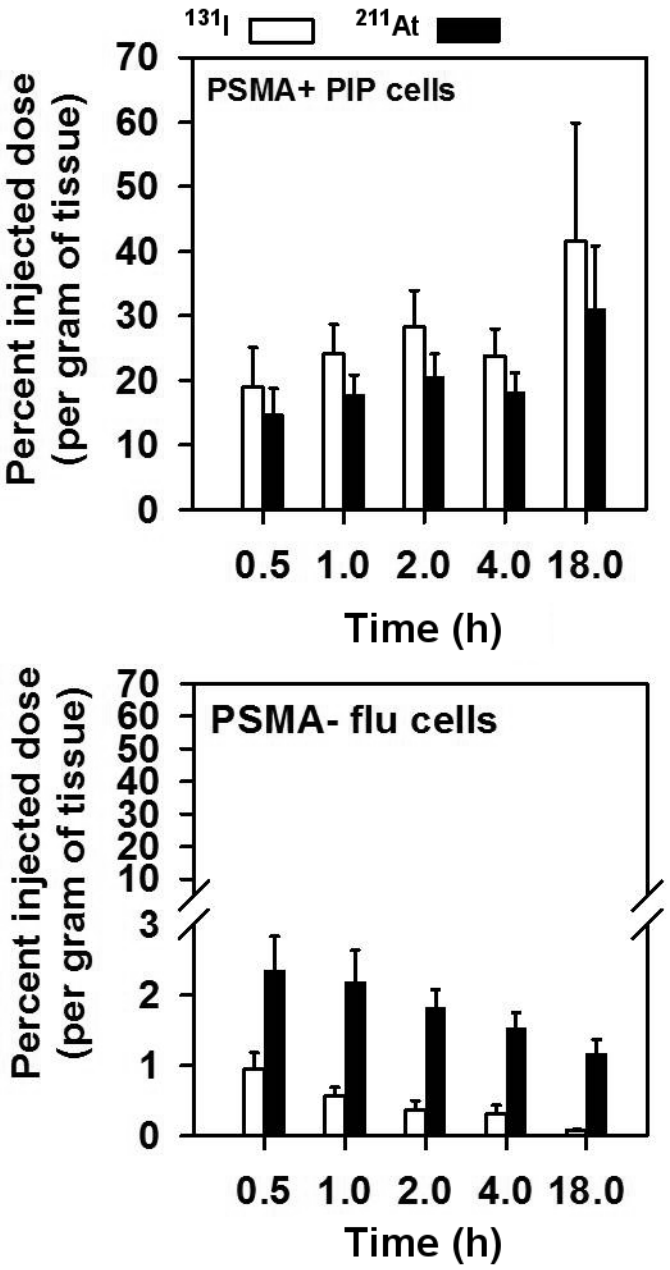

Figure 2. Uptake of ^{131}I and ^{211}At in PSMA+ PC3 PIP and PSMA- PC3 flu xenografts after administration of 0.2 MBq [^{131}I]**5** and [^{211}At]**6** in athymic mice. Values indicate mean ± standard deviation.

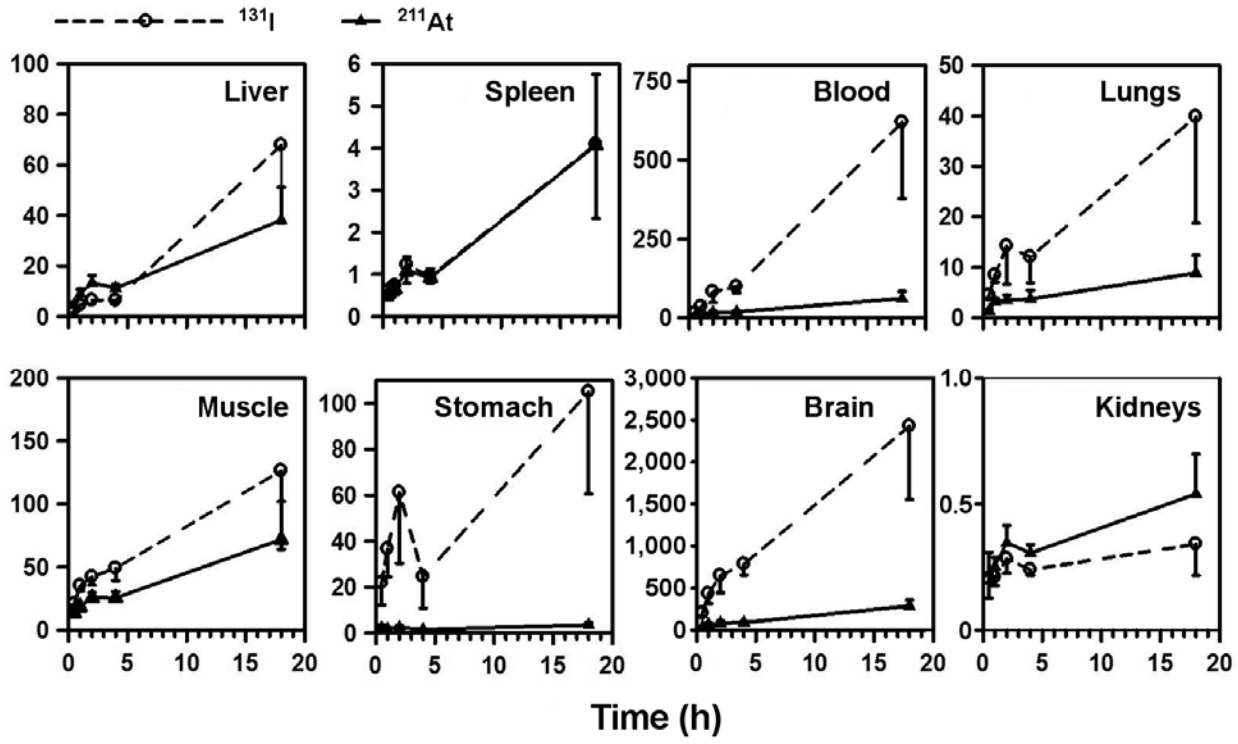

Figure 3. PSMA+ PC3 PIP tumor-to-tissue ratios after administration of 0.2 MBq [^{131}I]**5** and [^{211}At]**6** in athymic mice. Values indicate mean ± standard deviation.

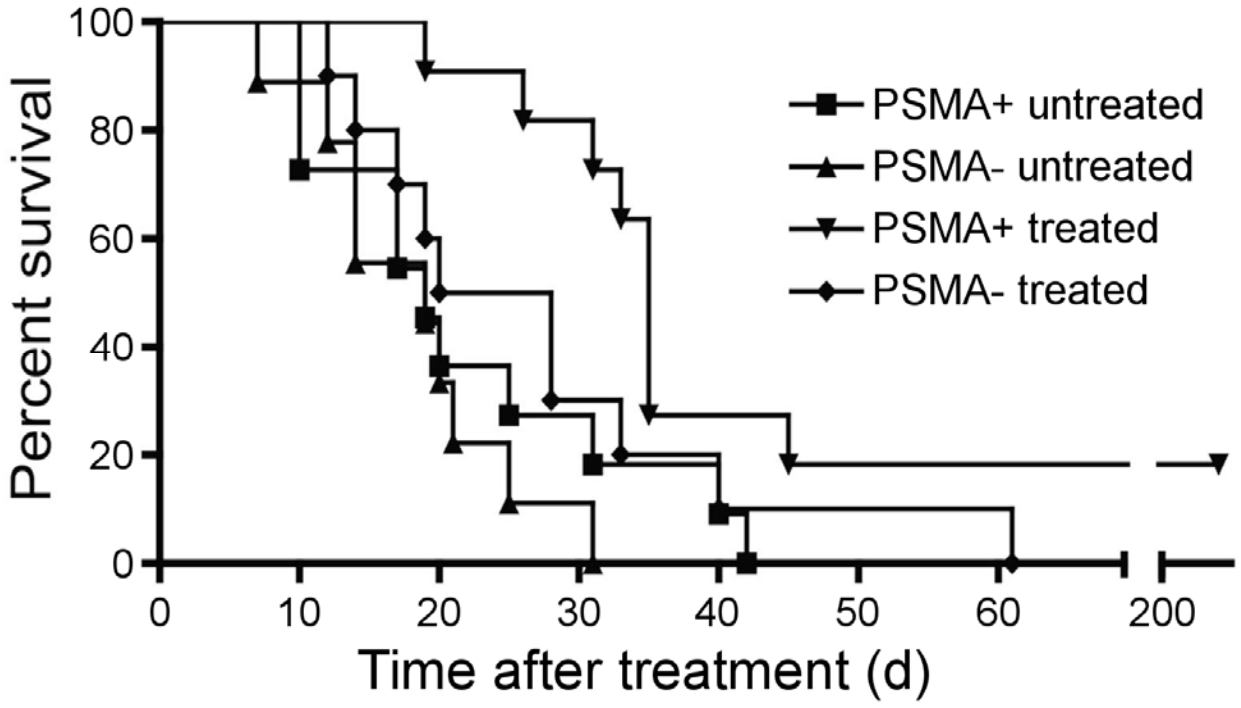

Figure 4. [^{211}At]**6** showed significant tumor growth delay in a flank xenograft model. Kaplan-Meier curve illustrating time for flank tumors to grow 10-fold in volume in athymic mice after 740 kBq [^{211}At]**6** treatment or control.

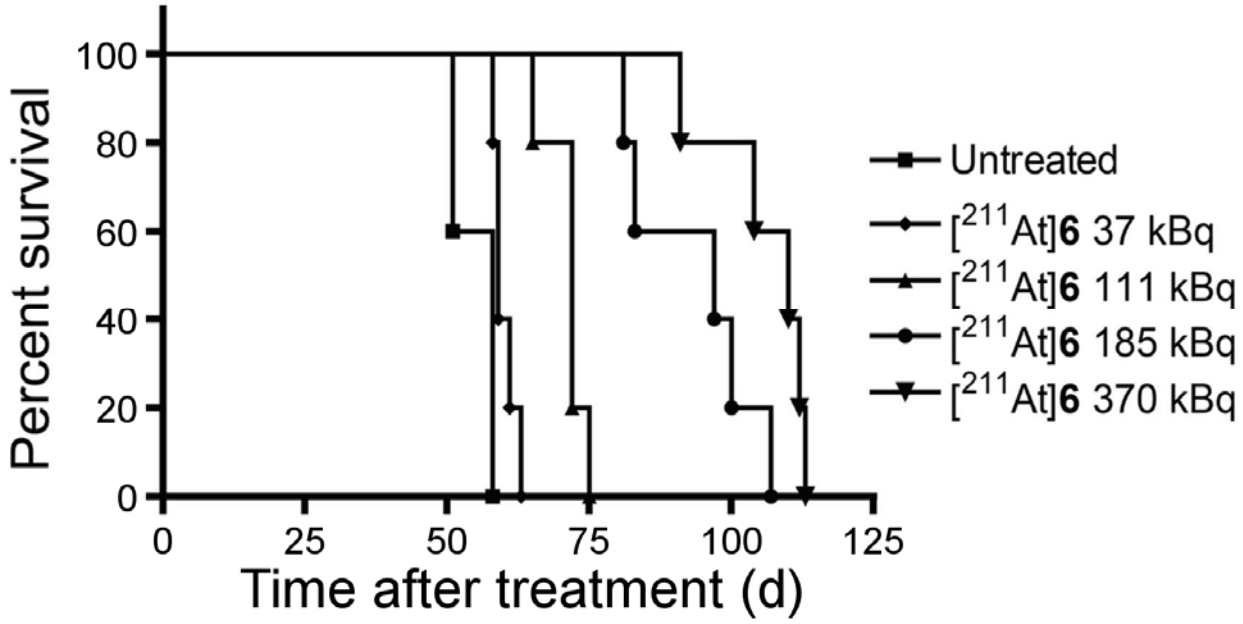

Figure 5. [^{211}At]**6** showed significant improvement in survival in a micrometastatic model. Kaplan-Meier curve showing survival time after treatment.

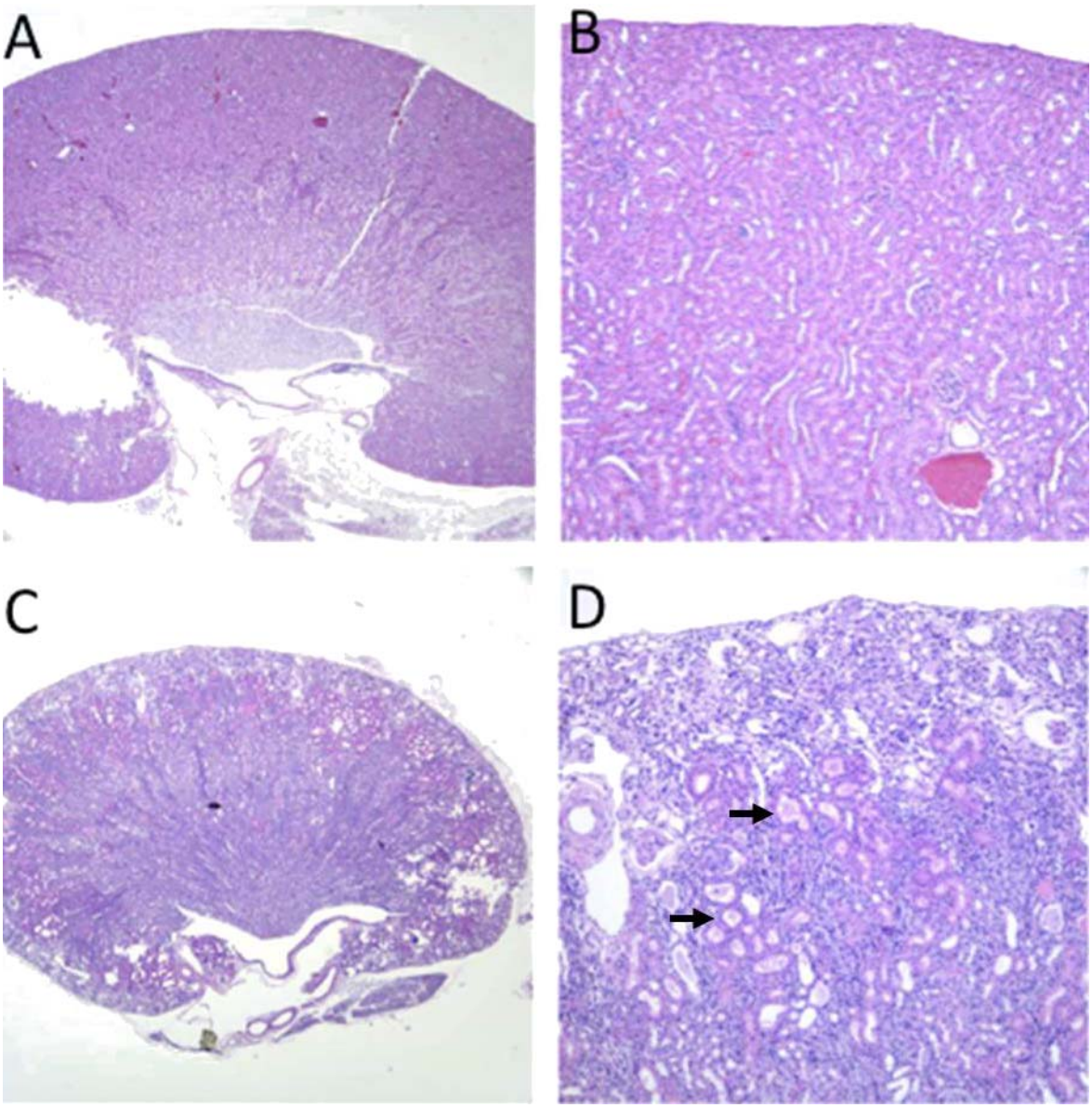

Figure 6. Renal histopathology from a non-treated mouse (**A**, **B**) and a mouse treated with 1.5 MBq [^{211}At]**6** (**C**, **D**). Treated kidney showed subcortical atrophy and degenerative loss of proximal tubules (arrows) consistent with late nephropathy due to α particle irradiation. **A**, **C**: 2×; **B**, **D**: 10×.

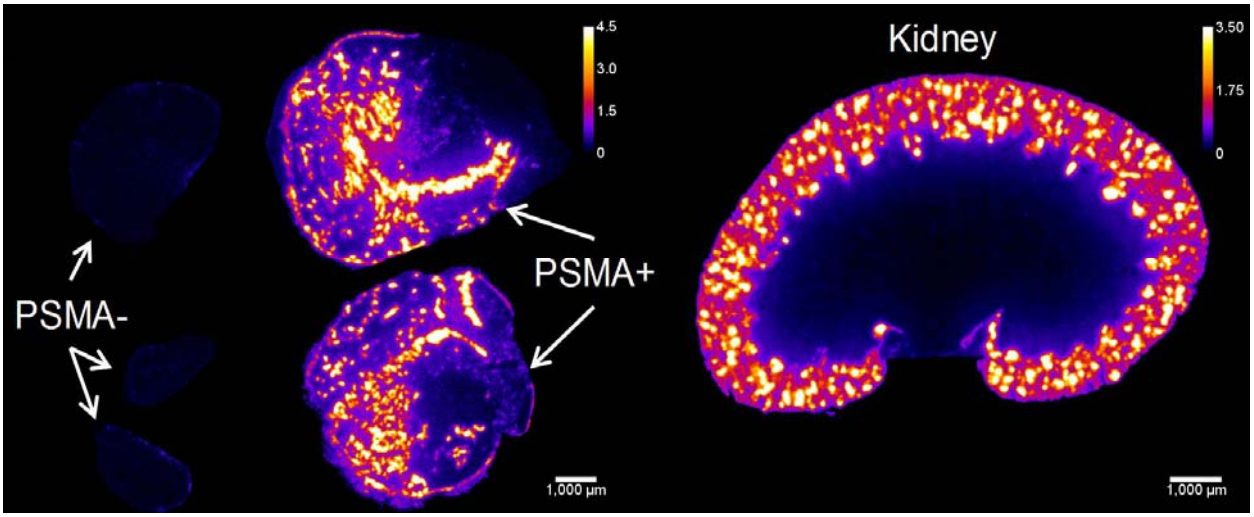

Figure 7. α-Camera images at 1 h showing relative [^{211}At]**6** activity concentrations for PSMA+ and PSMA- tumors, and kidneys. Scale shows activity concentration relative to whole tumor/kidney average concentration. White bar = 1 mm.